Improved Metal Artifact Reduction via Image Quality Metric Optimization

Michael Manhart, Marios Psychogios, Nadine Amelung, Michael Knauth, Christopher Rohkohl

***Abstract*—Cone-beam CT images acquired with C-arm systems are frequently disturbed by metal artifacts. Recently, correction algorithms based on the normalized metal artifact reduction (NMAR) algorithm were introduced for commercial C-arm systems enabling restoration of most part of soft tissue contrast. The NMAR algorithm replaces attenuation values of rays passing through metal by interpolation in projection domain. Since interpolation is imperfect and can cause inconsistencies, residual streak and shadow artifacts are often visible even after NMAR reconstruction. We introduce a novel iterative post-processing step for the NMAR algorithm which modifies the interpolated attenuation values by optimizing an image quality metric in the reconstructed volume to reduce residual artifacts. The novel approach was able to reduce residual artifacts on all 14 evaluated clinical neuroradiology datasets with only moderate increase of computation time (average +12 s).**

I. Introduction

Flat-detector CT (FD-CT) with C-arm systems is frequently acquired after interventional procedures for assessing treatment success and checking for complication, e.g. cerebral bleeding in neuroradiological interventions [1]. However, in many interventions metallic devices like coils are implanted or highly attenuating embolization material like Onyx is used. These materials cause severe streak and shadow artifacts in the reconstructed volume and impede diagnostic image quality. Recently, metal artifact reduction (MAR) techniques based on the normalized metal artifact reduction (NMAR) algorithm [2] were introduced for commercial C-arm systems, which are able to restore diagnostic image quality and have computation times suitable for interventional procedures [3], [4]. The NMAR algorithm starts with an initial reconstruction of an uncorrected volume. By thresholding operations a metal volume and a prior volume with tissue, air and bone structures are extracted. Then, metal masks in the projection images are computed by forward projection of the metal volume and normalized projection images are computed by dividing the projection images by forward projections of the prior volume. The masked metal in the normalized projections is removed by interpolation, the corrected projections are denormalized and the NMAR volume is reconstructed. The advantage of the normalization in NMAR is that edges from high-contrast objects like bones are restored in the interpolated metal shadow and details close to the metal object are better preserved [2]. Nevertheless, clinical experience showed that some disturbing residual streak and shadow artifacts are frequently still visible in reconstructed volumes. We present a novel iterative framework applicable after NMAR reconstruction, which reduces residual artifacts in a clinically applicable computation time. The framework optimizes an image quality metric (IQM) of the reconstructed volume (e.g., total variation (TV) [5]) by modifying the interpolated attenuation values of rays passing through the metal object.

M. Manhart and C. Rohkohl are with Siemens Healthcare GmbH, Advanced Therapies, Forchheim, Germany. M. Psychogios, N. Amelung, and M. Knauth are with Department of Neuroradiology, Universitätsmedizin Göttingen, Göttingen, Germany.
Email: michael.manhart@siemens.com

II. Materials & Methods

A. Clinical MAR Framework

Due to the severe metal artifacts in many clinical FD-CT images, the computation of the prior image by simple multilevel thresholding as in the original NMAR algorithm is not practical. Thus, we use an alternative approach to extract the prior image. First, an uncorrected volume is reconstructed, metal objects are extracted by a dedicated automated segmentation algorithm and projection metal masks are computed by forward projection. The metal is removed by interpolation and a first corrected volume is reconstructed, which is then used as the prior volume in a secondary NMAR reconstruction. Finally, the IQM optimization technique discussed below is applied to remove residual artifacts.

B. Mathematical Derivation of Optimization Algorithm

1) Notation: The reconstruction problem is denoted by volume $\hat{\mathbf{v}} \in \mathbb{R}^N$, measured line integrals $\hat{\mathbf{p}} \in \mathbb{R}^M$ and the system matrix $\hat{\mathbf{A}} \in \mathbb{R}^{M\times N}$ indicating the contribution of voxel i to line integral j

$$\hat{\mathbf{p}} = \hat{\mathbf{A}}\hat{\mathbf{v}} \qquad \hat{p}_j = \sum_{i=1}^{N} \hat{v}_i \hat{a}_{ji}. \tag{1}$$

The volume $\hat{\mathbf{v}}$ can be reconstructed using a filtered-backprojection (FBP) algorithm [6] by backprojection of weighted and filtered line integrals $\hat{\mathbf{f}} \in \mathbb{R}^M$

$$\hat{\mathbf{v}} = \tilde{\mathbf{A}}^T\mathbf{W}\hat{\mathbf{p}} = \tilde{\mathbf{A}}^T\hat{\mathbf{f}} \qquad \mathbf{W} \in \mathbb{R}^{M\times M}, \tag{2}$$

where matrix $\mathbf{W}$ describes the weighting and filtering matrix and $\tilde{\mathbf{A}}^T$ the backprojection matrix with the corresponding backprojection weights of the FBP algorithm. In case of NMAR the values of $\mathbf{p}$ inside the metal shadow are estimated by interpolation, might be inconsistent and cause residual artifacts. Our goal is to correct the filtered data $\hat{\mathbf{f}}$ to reduce these inconsistencies. We assume that inconsistencies caused by interpolation in $\hat{\mathbf{p}}$ have only local influence on the filtered

DOI: 10.12059/Fully3D.2017-11-3202038

data $\hat{\mathbf{f}}$. Thus, we restrict the problem to the filtered data $\mathbf{f} \in \mathbb{R}^m$, $m \ll M$ containing only the m values inside or spatially close to the metal shadows and to the voxels $\mathbf{v} \in \mathbb{R}^n$, $n < N$ influenced by the filtered values in $\mathbf{f}$. The matrix $\mathbf{A} \in \mathbb{R}^{m \times n}$ describing the relation between $\mathbf{f}$ and $\mathbf{v}$ is build from the corresponding entries in $\tilde{\mathbf{A}}$. Furthermore, we denote the corresponding voxel values from the initial NMAR reconstruction by $\mathbf{v}_0 \in \mathbb{R}^n$. The IQM is a convex and differentiable function denoted by $F : \mathbb{R}^n \rightarrow \mathbb{R}_0^+$ mapping $\mathbf{v}$ to a non-negative scalar which increases with the strength of artifacts in the volume (e.g., total variation).

2) Problem Formulation: Our goal is to find filtered data $\mathbf{f}_{\text{opt}} \in \mathbb{R}^m$ with less inconsistencies by adding correction values $\mathbf{s}_{\text{opt}} \in \mathbb{R}^m$ to the filtered NMAR data $\mathbf{f}$

$$\mathbf{f}_{\text{opt}} = \mathbf{f} + \mathbf{s}_{\text{opt}}. \tag{3}$$

When correction values $\mathbf{s} \in \mathbb{R}^m$ are added to $\mathbf{f}$, the corresponding voxel values in the reconstructed volume are given by

$$\mathbf{v}(\mathbf{s}) = \mathbf{v}_0 + \mathbf{A}^T \mathbf{s}. \tag{4}$$

To find the optimized correction values $\mathbf{s}_{\text{opt}}$, we minimize the IQM evaluated on the updated volume voxels $\mathbf{v}(\mathbf{s})$

$$\mathbf{s}_{\text{opt}} = \text{argmin}_{\mathbf{s}}\, F(\mathbf{v}(\mathbf{s})) \qquad F(\mathbf{v}(\mathbf{s})) : \mathbb{R}^m \rightarrow \mathbb{R}^n \rightarrow \mathbb{R}_0^+. \tag{5}$$

By inserting Equation 4 in Equation 5 the optimization problem results in

$$\mathbf{s}_{\text{opt}} = \text{argmin}_{\mathbf{s}}\, F\left(\mathbf{v}_0 + \mathbf{A}^T \mathbf{s}\right). \tag{6}$$

3) Gradient Descent Optimization: As F is a convex function, Equation 6 can be solved using a gradient descent scheme with line search [7]. The gradient decent algorithms applies iterative updates

$$\mathbf{s}_k = \mathbf{s}_{k-1} - \alpha_k \nabla \mathbf{F}_k,\, k \in \mathbb{N}$$

with step size $\alpha_k \in \mathbb{R}^+$ until the minimum at $\mathbf{s}_{\text{opt}}$ is found. To apply the gradient descent scheme, the gradient $\nabla \mathbf{F}$ of the IQM w.r.t. to the correction values $\mathbf{s}$ is needed. Furthermore, an appropriate step size α_k must be determined for each iteration.

Gradient Computation: The gradient of F w.r.t. $\mathbf{s}$ is denoted by $\nabla \mathbf{F} = \left(\frac{\partial F}{\partial s_1}, \cdots, \frac{\partial F}{\partial s_m}\right)^T$. The partial derivatives $\frac{\partial F}{\partial s_j}$ can be derived via the chain rule of differentiation and Equation 1

$$\frac{\partial F}{\partial s_j} = \sum_{i=1}^{n} \frac{\partial F}{\partial v_i} \frac{\partial v_i}{\partial s_j} = \sum_{i=1}^{n} \frac{\partial F}{\partial v_i} a_{ji}, \tag{7}$$

$$\nabla \mathbf{F} = \mathbf{A} \frac{\partial F}{\partial \mathbf{v}}. \tag{8}$$

Equation 8 shows that $\nabla \mathbf{F}$ is calculated by computing the gradient of F w.r.t. to the voxel values and forward projection via $\mathbf{A}$.

Line Search: An appropriate α_k can be determined by line search

$$\alpha_k = \text{argmin}_{\alpha \in \mathbb{R}^+} F\left(\mathbf{v}_0 + \mathbf{A}^T \left(\mathbf{s}_{k-1} - \alpha \nabla \mathbf{F}_k\right)\right) \tag{9}$$

With $\mathbf{v}_{k-1} = \mathbf{v}_0 + \mathbf{A}^T \mathbf{s}_{k-1}$ denoting the resulting volume of the previous iteration step and $\nabla \mathbf{v}_k = \mathbf{A}^T \nabla \mathbf{F}_k$ denoting the backprojected gradient, we reformulate Equation 9

$$\alpha_k = \text{argmin}_{\alpha \in \mathbb{R}^+} F\left(\mathbf{v}_{k-1} - \alpha \nabla \mathbf{v}_k\right). \tag{10}$$

Thus, the line search can be computed completely in the volume domain and only an initial backprojection operation to compute $\nabla \mathbf{v}_k$ is required.

C. Image Quality Optimization Framework

Based on the results of Equation 8 and 10 the optimization framework shown in Figure 1 is derived. In this work, the well-known TV [5] is used as IQM. However, the framework supports any convex IQM where a gradient w.r.t. voxel values can be computed. As input for the framework serves the initially reconstructed volume using NMAR including the metal masks in volume and projection domain. In step 1 the soft tissue voxels potentially affected by metal artifacts (i.e., soft tissue voxels in slices with or close to metal objects) are segmented by thresholding. These soft tissue voxels are used in the subsequent iterative IQM optimization. Step 2 computes the gradient of the TV norm [8] w.r.t. to $\mathbf{v}$ on the segmented voxels. In step 3 the IQM gradient w.r.t. the correction values $\mathbf{s}$ is computed by forward projection of the volumetric gradient on to the metal shadow (see Equation 8). In step 4, the IQM gradient w.r.t. $\mathbf{s}$ is backprojected on to the segmented voxels to compute a volumetric IQM gradient w.r.t. $\mathbf{s}$. As shown by Equation 10 this allows to find an appropriate step size by line search in step 5 without any further computational expensive projection steps. The line search is conducted by back tracking line search [7]. Then the volume is updated with volumetric gradient and the found optimal step size. Finally, Step 6 checks for stopping criterion. In this work we always stop after a fixed number of 10 iterations. The general framework was implemented using C++ programming language, the forward- and backprojection operations [9] as well as the TV and TV gradient computation were implemented using CUDA GPU programming language.

III. Clinical Evaluation

A. Clinical Datasets

We evaluated the proposed optimization framework with 14 clinical FD-CT datasets acquired using an Artis Q angiography system (Siemens Healthcare GmbH, Germany). A dedicated head soft tissue contrast protocol was used with 20 s acquisition time, 496 projections, 200° angular range, tube voltage 109 kV and a dose of $1.8\,\mu$Gray per projection. All datasets contain a single or multiple highly attenuating objects like metal coils or Onyx embolization material causing extensive streak and shadow artifacts in volumes reconstructed without MAR. All datasets were reconstructed using a proprietary

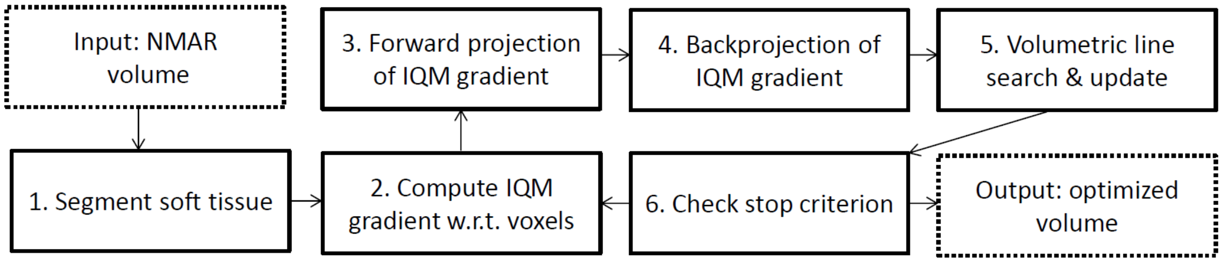

Figure 1. Flowchart of IQM optimization framework.

exact FBP-type reconstruction software without any MAR, using NMAR and using NMAR plus the proposed additional optimization step (NMAR+OPT).

B. Qualitative Evaluation

For qualitative evaluation the reconstruction of all datasets using NMAR was compared to NMAR+OPT by a user experienced with FD-CT imaging. The improvements from NMAR to NMAR+OPT were rated in a range from 0 (no improvement) to 3 (strongest improvement). Figure 2 shows example slices with corresponding ratings. From the 14 datasets, 3 achieved rating 1, 5 rating 2 and 6 rating 3 and the average rating was 2.2. The additional optimization was beneficial in all datasets and no degeneration in image quality by NMAR+OPT was found.

C. Computation Time

The reconstructions were computed on a dedicated clinical workstation with Intel® Xeon® processor E5-1650 with 6 cores and 3.20 GHz, 32 GB RAM and NVIDIA® Quadro® K5000 GPU with 4 GB GPU RAM. The computation time for the additional optimization step was measured for all clinical datasets and depends on the size of the metal object. The range of the computation time was between $4\,\mathrm{s}$ and $49\,\mathrm{s}$ with an average of $12\,\mathrm{s}$ and a median of $5.5\,\mathrm{s}$.

IV. Discussion & Conclusions

The NMAR [2] is able to improve diagnostic image quality in FD-CT datasets with metal artifacts [3] and is a very valuable technique for interventional FD-CT imaging [4]. However, some disturbing streak and shadow artifacts are often still visible in soft tissue imaging. These artifacts are caused by the imperfect interpolation of the attenuation values in the metal shadow. To further reduce residual artifacts, we introduce an iterative framework as an additional post-processing step for the NMAR algorithm. The framework adjusts the filtered attenuation values inside the metal shadow such that an image quality metric (IQM) determined on the reconstructed soft tissue is optimized. The derived iterative framework is computationally efficient since the problem dimension can be reduced to projection values in the metal shadow and voxels in metal artifact affected slices. Furthermore, the framework allows to determine an optimal step size in each iteration via line search in volume domain. This avoids the problem in general iterative reconstruction algorithms to determine an appropriate step size providing convergence guarantee and speed. We use total variation [5] as IQM, however, it is possible to use other convex and differentiable IQMs within the framework. The proposed framework successfully reduced residual artifacts in an evaluation with 14 clinical FD-CT head datasets with only a moderate computational complexity compared to fully iterative reconstruction approaches (average additional computation time was $12\,\mathrm{s}$). One limitation of this work is the clinical evaluation which was not blinded and included only a limited number of datasets. In future studies a more extensive and blinded clinical evaluation is desired, also with datasets from other body regions (e.g., liver). Furthermore, alternative IQMs like the image histogram entropy and improved stopping criterion could be evaluated.

Disclaimer: The concepts and information presented in this paper are based on research and are not commercially available.

References

[1] J. Leyhe, I. Tsogkas, A. Hesse, D. Behme, K. Schregel, I. Papageorgiou, J. Liman, M. Knauth, and M. Psychogios, "Latest generation of flat detector CT as a peri-interventional diagnostic tool: a comparative study with multidetector CT," *J Neurointerv Surg*, 2016, published Online First: 20 December 2016. doi: 10.1136/neurintsurg-2016-012866.

[2] E. Meyer, R. Raupach, M. Lell, B. Schmidt, and M. Kachelrieß, "Normalized metal artifact reduction (NMAR) in computed tomography," *Medical Physics*, vol. 37, no. 10, pp. 5482–5493, 2010.

[3] A. Mennecke, S. Svergun, B. Scholz, K. Royalty, A. Dörfler, and T. Struffert, "Evaluation of a metal artifact reduction algorithm applied to post-interventional flat detector CT in comparison to pre-treatment CT in patients with acute subarachnoid haemorrhage," *European Radiology*, vol. 27, no. 1, pp. 88–96, 2016.

[4] M.-N. Psychogios, B. Scholz, C. Rohkohl, Y. Kyriakou, A. Mohr, P. Schramm, D. Wachter, K. Wasser, and M. Knauth, "Impact of a new metal artefact reduction algorithm in the noninvasive follow-up of intracranial clips, coils, and stents with flat-panel angiographic CTA: initial results," *Neuroradiology*, vol. 55, no. 7, pp. 813–818, 2013.

[5] L. I. Rudin, S. Osher, and E. Fatemi, "Nonlinear total variation based noise removal algorithms," *Physica D: Nonlinear Phenomena*, vol. 60, no. 1, pp. 259–268, 1992.

[6] G. L. Zeng, *Medical Image Reconstruction: A Conceptual Tutorial*, 1st ed. Berlin, Germany: Springer, 2010.

[7] S. Boyd and L. Vandenberghe, *Convex Optimization*. Cambridge University Press, 2004.

[8] P. T. Lauzier, J. Tang, and G.-H. Chen, "Prior image constrained compressed sensing: Implementation and performance evaluation," *Medical Physics*, vol. 39, no. 1, pp. 66–80, 2012.

[9] B. Keck, H. Hofmann, H. Scherl, M. Kowarschik, and J. Hornegger, "GPU-accelerated SART reconstruction using the CUDA programming environment," in *SPIE Medical Imaging*. Lake Buena Vista, FL, USA: International Society for Optics and Photonics, February 2009, pp. 72 582B1–72 582B9.

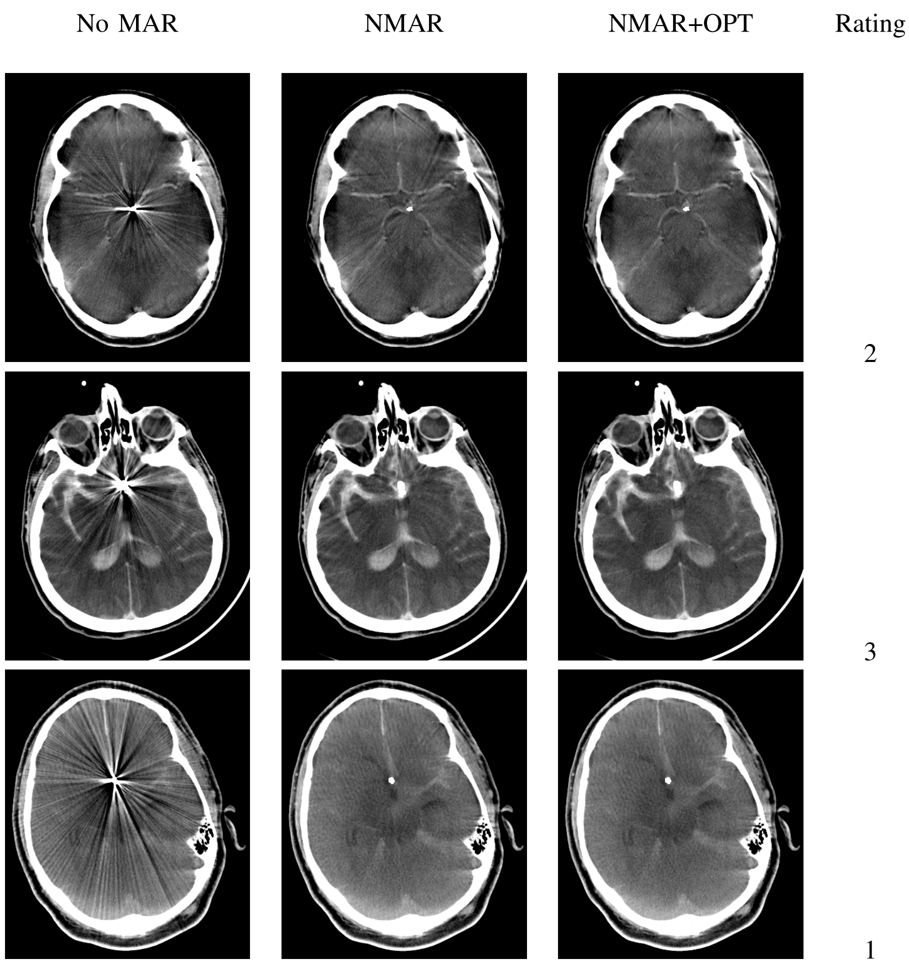

Figure 2. FD-CT head images with metal objects reconstructed without MAR (left), with NMAR (center) and with NMAR+OPT (right). The right column shows the NMAR vs. NMAR+OPT improvement rating. Window [-50 150] HU, slice thickness 5 mm.